






Article

Corrosion of Titanium Alloys Anodized Using Electrochemical Techniques

Jesús Manuel Jáquez-Muñoz ¹, Citlalli Gaona-Tiburcio ¹, Ce Tochtli Méndez-Ramírez ^{2,*}, Miguel Ángel Baltazar-Zamora ², Francisco Estupinán-López ¹, Raul German Bautista-Margulis ³, Josefina Cuevas-Rodríguez ², Juan Pablo Flores-De los Rios ⁴ and Facundo Almeraya-Calderón ^{1,*}

¹ Universidad Autónoma de Nuevo León, FIME, Centro de Investigación e Innovación en Ingeniería Aeronáutica (CIIA), San Nicolás de los Garza 66455, Mexico

² Facultad de Ingeniería Civil/Facultad de Arquitectura, Universidad Veracruzana, Xalapa 91000, Mexico

³ División Académica de Ciencias Biológicas, Universidad Juárez Autónoma de Tabasco, Villahermosa 86040, Mexico

⁴ Tecnológico Nacional de Mexico-Instituto Tecnológico de Chihuahua, Av. Tecnológico 2909, Chihuahua 31130, Mexico

* Correspondence: cmendez@uv.mx (C.T.M.-R.); facundo.almerayacl@uanl.edu.mx (F.A.-C.)

Abstract: The anodization of titanium has been an excellent option for protecting titanium and its alloys from corrosive environments such as acids and chloride systems, by generating a homogenous oxide layer. The objective of the current investigation was to evaluate the electrochemical corrosion behavior of alloys Ti-6Al-2Sn-4Zr-2Mo and Ti-6Al-4V anodized in 1M H₂SO₄ and H₃PO₄ solutions at a current density of 2.5×10^{-3} A/cm². The anodization's electrochemical characterization was achieved in NaCl and H₂SO₄ at 3.5% wt. electrolytes. Scanning electron microscopy (SEM) was employed to determine the anodized thickness and morphology. Cyclic potentiodynamic polarization (CPP) and electrochemical impedance spectroscopy (EIS), based on ASTM G61-86 and G106-15 Standards, were the electrochemical techniques mainly employed. The anodized samples presented a change in E_{corr} values and a higher passivation zone. The EIS plot showed a higher resistance for samples anodized in H₃PO₄ and Ti-6Al-2Sn-4Zr-2Mo.

Keywords: titanium; anodized; corrosion; electrochemical impedance spectroscopy; Warburg's diffusion



Citation: Jáquez-Muñoz, J.M.; Gaona-Tiburcio, C.; Méndez-Ramírez, C.T.; Baltazar-Zamora, M.Á.; Estupinán-López, F.; Bautista-Margulis, R.G.; Cuevas-Rodríguez, J.; Flores-De los Rios, J.P.; Almeraya-Calderón, F. Corrosion of Titanium Alloys Anodized Using Electrochemical Techniques. *Metals* **2023**, *13*, 476. <https://doi.org/10.3390/met13030476>

Academic Editor: Mosab Kaseem

Received: 30 January 2023

Revised: 19 February 2023

Accepted: 19 February 2023

Published: 24 February 2023



Copyright: © 2023 by the authors. Licensee MDPI, Basel, Switzerland. This article is an open access article distributed under the terms and conditions of the Creative Commons Attribution (CC BY) license (<https://creativecommons.org/licenses/by/4.0/>).

1. Introduction

Industries, including biomedicine and aerospace, require materials such as titanium for their great properties, both mechanical and chemical. For this reason, the study of the oxide layer produced on titanium has increased in recent years, with a view to increasing the life of components, reducing costs for preventive and corrective maintenance, and replacing steel in zones where corrosion is the higher priority [1–3].

Nonetheless, titanium and its alloys can present degradation when exposed to chloride and acid media due to the defects in the layers generated by natural processes. Authors have reported that the oxide film generated by titanium is composed of multivalent titanium, which provokes layer degradation by galvanic or crevice corrosion [4–6].

The classification of Ti-alloys can be divided into four classes: α , near to α , $\alpha + \beta$, and metastable β ; the classification will depend on the percentage of β elements that are present. Gloria et al. and Peters et al. [7,8] indicated that the β elements are mainly Mo, Cr, V, Ta, Fe, and Ni; the presence of these stabilizers can change the mechanical and chemical properties of alloys. Song et al. [9] related the presence of vanadium with a reduction in the oxide layer's corrosion resistance to vanadium dissolution. Furthermore, for biomedical applications, elements such as V and Al are classified as toxic for the human body because they provoke genotoxicity, Alzheimer's, and peripheral neuropathy [10,11].

A good option for the problems generated by vanadium dissolution is to employ alloys with elements such as Mo, Zr, Ta, or Sn. Mo and Ta are β stabilizers, so the properties generated by V can be substituted. Further, the properties of the passive layer will increase because authors have reported that alloys and passive layers with the presence of Mo increase the corrosion resistance and produce a layer that is more difficult to dissolve. Additionally, Mo presents a higher biocompatibility than V [12–14]. Alloys such as Ti-6Al-2Sn-4Zr-2Mo can be selected to substitute Ti-6Al-4V, due to the properties of Mo as a β stabilizer. Likewise, the chemical properties of Zr and Sn help to create a better passive layer, even for corrosion resistance and biocompatibility [15–17].

Titanium and its alloys are reactive to oxygen; the kinetics of oxidation occurs instantly and generate a TiO_2 protective layer, as indicated in the research by Rao, Sul and Wang [18–20]. Various surface treatments applied to generate an oxide layer on titanium to increase the corrosion resistance, such as sputtering, plasma, sol–gel, passivation, electrodeposition, and anodization, have been employed to obtain a passive layer [21–23]. Narayanan et al. and Jaquez-Muñoz et al. [24,25] found that anodizing could be considered one of the most important surface treatments due to the quality of the oxide layer, the easy manufacturing process, and the low production and operation costs.

Past research [26–30] demonstrated that the natural passive layer of titanium is susceptible to Cl^- ion attacks because the diffusion of Cl^- ions weakens the oxide layer. The presence of Cl^- and OH^- in passive materials increases the corrosion rates by interstitial penetration [31–34]. When electrochemical noise (EN) results were analyzed, anodized Ti-alloys showed that the pore size was directly related to the corrosion rate, and the anodized H_3PO_4 presented higher corrosion resistance due to H_2SO_4 creating bigger pores. Moreover, alloys with elements such as Mo, Zr, Sn, and Cr presented the best performance against corrosion. In the alloy Ti Beta-C, the performance was good, but the presence of V decreased the passive range of the material compared with materials that did not have V [26].

However, past researchers did not consider that the change in E_{corr} against the metal matrix and the electrochemical impedance spectroscopy (EIS) was more related to the thickness of the coating. Socorro-Perdomo et al. [35] obtained, in a Ti-Mo alloy, the presence of two different Randle circuits when samples were studied at different potentials. At passive potentials, two time constants were present and related to the presence of Mo with higher corrosion resistance.

Chávez-Díaz et al. [36] related the capacitive response with defects in passive oxides, mainly oxygen vacancies in the oxide layer, principally suboxides such as TiO , Ti_2O_3 , and Al_2O_3 , and the formation of oxyhydroxides and/or hydroxides. Mohazzab et al. [37] obtained one constant circuit for alloy without coating, and with the coatings' two time constants, they related with the porous layer and the substrate/coating interface.

A low capacitive response is related to the protective layer and indicates better corrosion properties. However, not all the samples presented the common double-layer equivalent circuit of resistance and capacitance. Some samples have inductance, and this behavior is shown when the species are adsorbed on the electrode surface. It occurs when the alloying elements help to grow the oxide layer [38]. Some authors interpreted with three RC constants, but the behavior was similar to the diffusion process and associated with different porosity layers [39].

In other research, a diffusion process occurs; this is interpreted as Warburg's element (W); when the resistance of W is high, it can be associated with the formation of oxide films [40]. Kulova et al. [41] related the W with the diffusion of sodium in the solid phase. Other authors related it to the diffusion of Cl^- , and when W impedance was decreased by the concentration of ions, the passive layer was damaged [42].

This work aims to study the electrochemical behavior of anodization on Ti-6Al-2Sn-4Zr-2Mo and Ti-6Al-4V exposed at 3.5 wt. % to NaCl and H_2SO_4 solutions. The electrochemical characterization was performed by cyclic potentiodynamic polarization (CPP) and elec-

trochemical impedance spectroscopy (EIS). The anodized layers were characterized by scanning electron microscopy (SEM).

2. Materials and Methods

2.1. Material

The materials used in this work were Ti-6Al-2Sn-4Zr-2Mo (Supra alloys, Camarillo, CA, USA) and, Ti-6Al-4V (Titanium Engineers, Stafford, TX, USA) used in the received condition. The chemical composition of these alloys was obtained by atomic absorption spectrometry and is listed in Table 1.

Table 1. Chemical composition of the titanium alloys (wt. %).

Elements	Ti-6Al-2Sn-4Zr-2Mo	Ti-6Al-4V
Ti	84.65 ± 0.19	87.71 ± 0.36
Al	6.75 ± 0.20	7.14 ± 0.37
Sn	2.08 ± 0.01	–
V	–	4.03 ± 0.08
Zr	4.18 ± 0.01	–
Mo	1.99 ± 0.008	–

2.2. Microstructural Characterization

Titanium alloys were prepared by metallography technique [43]. The materials were polished using various SiC sandpaper grades 400, 600, and 800; each sample was ultrasonically cleaned for 10 min in ethanol (C₂H₅OH) and deionized water. The samples were subjected to a chemical attack using a Kroll solution made up of 3 mL of hydrofluoric acid (HF), 5 mL of nitric acid (HNO₃), and 100 mL of water (H₂O) for 30 s [44].

The surface and cross-section of titanium alloys were investigated using secondary electron (SE) and backscattered electron (BSE) detectors in a scanning electron microscope (SEM, JEOL-JSM-5610LV, Tokyo, Japan) operating at 20 kV and 8.5 and 12 mm work distance. The chemical composition of alloys was obtained by energy-dispersive X-ray spectroscopy (EDS, JEOL-JSM-5610LV, Tokyo, Japan).

2.3. Anodizing Process

Ultrasonic cleaning in ethanol (C₂H₅OH) and deionized water served as the pretreatment for 10 min.

The anodizing procedure was carried out in an electrochemical cell with a graphite rod serving as the cathode and 1 M electrolytes (analytical grade reagents (JT Baker)), with the anodizing electrolyte's temperature being 25 °C ± 1. Using a DC power source, the titanium samples' current density was 2.5 × 10^{−3} A·cm^{−2} for 600 s (XLN300025-GL). The AMS2487 specification was followed during the anodizing procedure [45].

2.4. Electrochemical Measurements

Cyclic potentiodynamic polarization (CPP) and electrochemical impedance spectroscopy (EIS) were carried out at room temperature using a VersaSTAT 4 Princeton Applied Research (Ametek, Inc. Oak Ridge, TN, USA) in 3.5 wt. % NaCl and H₂SO₄ solutions. A conventional three-electrode cell configuration was employed for electrochemical characterization at room temperature and all the corrosion tests were performed in triplicate. The working electrode (WE, with an exposed surface of 1 cm²) was anodized for the current study, the reference electrode (RE) was saturated calomel (SCE), and the counter electrode (CE) of platinum [46].

The CPP parameters were a scan potential from −1.2 to 1.2 V vs. SCE of OCP. The potential sweep was 1 mV/s to complete 1 cycle [47].

EIS was realized with a potential amplitude of ± 10 mV; the frequencies were from 100 kHz to 10 mHz. The equivalent circuit analysis was made in ZView [48].

3. Results

3.1. SEM Microstructural Analysis

Figure 1 shows the microstructure of the initial samples in the superficial section of Ti-6Al-2Sn-4Zr-2Mo and Ti-6Al-4V. Figure 1a shows Ti-6Al-2Sn-4Zr-2Mo, presenting α phase grains deformed with triple junction zones for β phase. Ti-6Al-4V had an equiaxial and fine grain, the β phase had a spherical form, and α was the matrix.

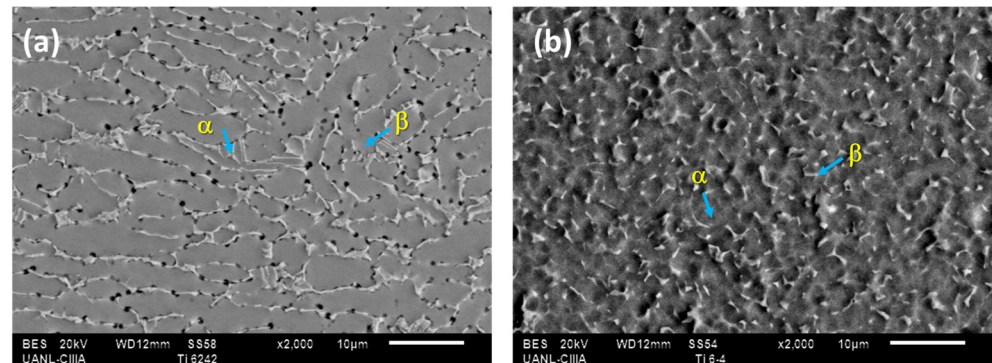


Figure 1. Micrograph obtained by SEM-BES: (a) Ti-6Al-2Sn-4Zr-2Mo and (b) Ti-6Al-4V.

3.2. SEM Surface Analysis of Anodized Alloys

Figure 2 shows the surface characterization of the samples anodized in H_2SO_4 and H_3PO_4 . Figure 2a shows the Ti-6Al-2Sn-4Zr-2Mo anodized in H_2SO_4 ; this sample presented a homogenous porosity, and the different levels can be observed, associated with a high rugosity. Figure 2b of Ti-6Al-4V anodized in H_2SO_4 shows lower porosity but little crack zones at a different level, associating this with high rugosity. Samples anodized in H_3PO_4 showed similar morphology with great porosities and heterogenous distribution and size.

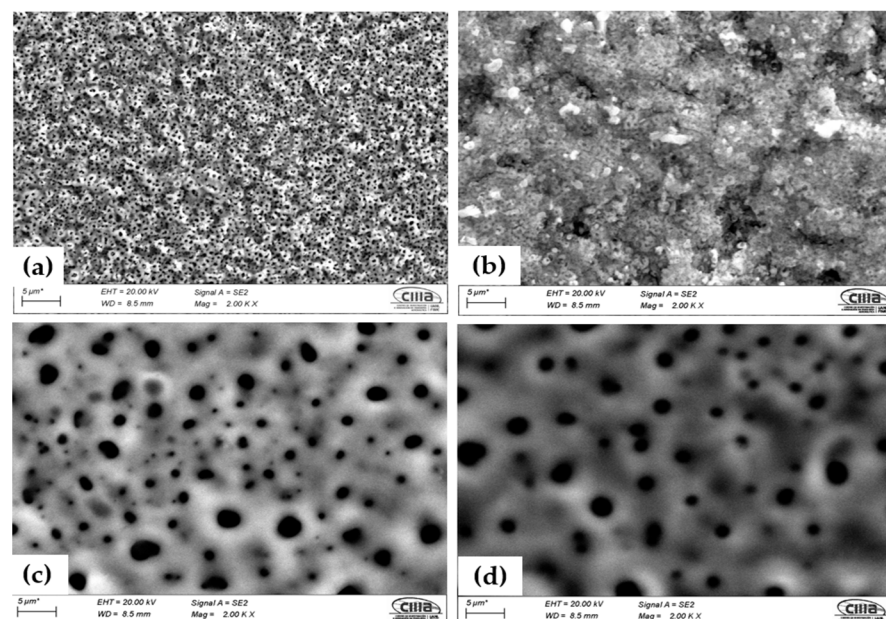


Figure 2. Micrographs of the anodized samples by SEM-SE. The sample anodized in H_2SO_4 (a) Ti-6Al-2Sn-4Zr-2Mo and (b) Ti-6Al-4V; in H_3PO_4 (c) Ti-6Al-2Sn-4Zr-2Mo and (d) Ti-6Al-4V.

3.3. SEM Cross-Section Analysis of Anodized Alloys

Figure 3 shows the cross-section of the anodized samples with the measurements and an element mapping by EDS for Ti-6Al-2Sn-4Zr-2Mo. Figure 3a shows the anodized sample in H_2SO_4 , where the average anodized thickness was $1.62 \mu\text{m}$, with a major thickness of $1.88 \mu\text{m}$ and a lower one of $1.36 \mu\text{m}$, having a uniform and continuous coating. At the top, the material's roughness can be observed, and cracks were not present. Figure 3b shows the anodization in H_3PO_4 , where the average anodized coating was $1.65 \mu\text{m}$ higher than that anodized in H_2SO_4 . However, this anodization presents more variability in the thickness with a lower measurement of $1.28 \mu\text{m}$ and a higher one of $2.08 \mu\text{m}$. However, the thickness of the sample is within the specifications of AMS2487B.

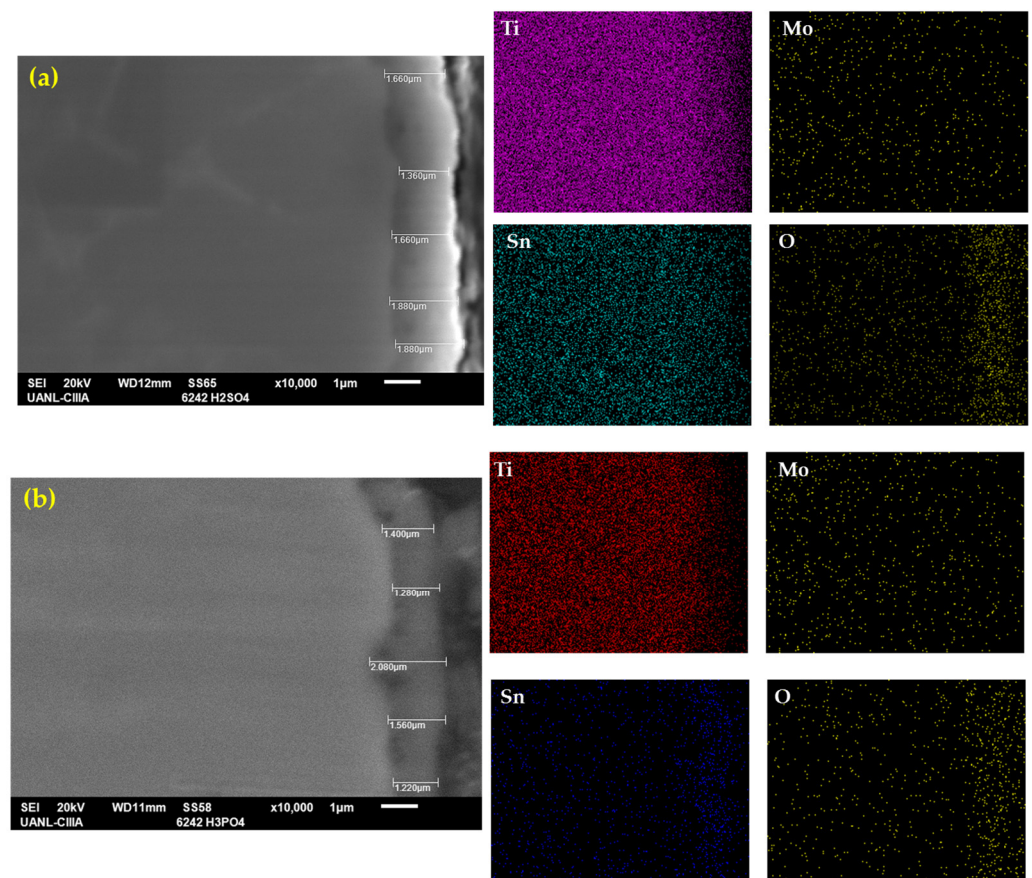


Figure 3. SEM-SEI of the cross-section of Ti-6Al-2Sn-4Zr-2Mo in (a) H_2SO_4 and (b) H_3PO_4 ; the elemental mapping by SEM identified Ti, Mo, Sn, and O.

For that reason, the porosities of Figure 2a,b could be localized at the top, but after that, a compact oxide layer was present. The element mappings of Figure 3 showed the presence of alloying elements. In the coating, titanium was localized in all alloys, but in the coating zone, the top was reduced; elements such as Sn had a presence in all the samples, including the top. The oxygen in Figure 3 is concentrated in the coating zone, relating that result to the oxide layer of Ti.

Figure 4 shows the cross-section of anodized Ti-6Al-4V with the measurements and the mapping of the chemical composition obtained by EDS. Figure 4a shows the sample anodized in H_2SO_4 , where the average anodized thickness was $0.95 \mu\text{m}$, with a higher thickness of $1.02 \mu\text{m}$ and a lower one of $0.88 \mu\text{m}$. This coating also presented a high roughness, and the morphology could not be related to a compact layer. Figure 4b shows the H_3PO_4 anodization had a higher coating thickness than the Figure 4a sample, with an average of $1.53 \mu\text{m}$. This coating also presented a higher thickness, and the layer was

compact. In some anodized zones, some discontinuities could be observed. Only the sample anodized in H_3PO_4 achieved the AMS2487B specs.

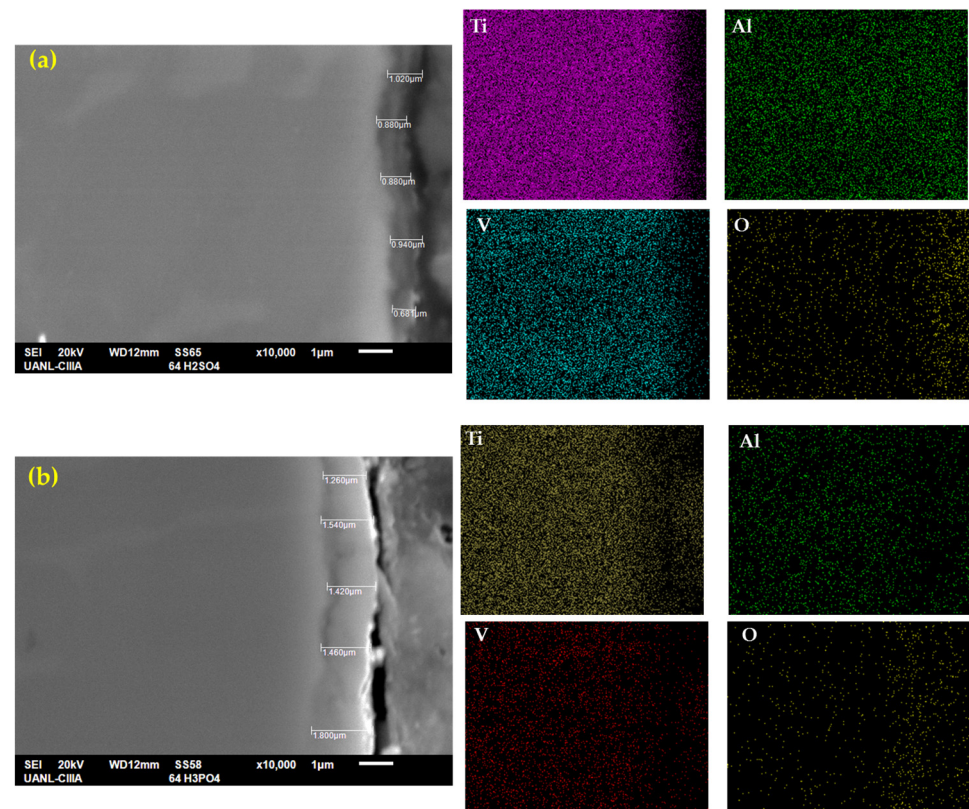


Figure 4. SEM-SEI of the cross-section of Ti-6Al-4V in (a) H_2SO_4 and (b) H_3PO_4 ; the elemental mapping by SEM identified Ti, Al, V, and O.

Figure 4a,b show the presence of the chemical elements. Titanium was also present in all matrixes, but the coating had more presence at the bottom than at the top for both samples. These anodized samples showed the presence of aluminum and vanadium (more than in the H_2SO_4 coating). This behavior is related to the formation of secondary oxides. Oxygen had a presence in the coating zone, as previously explained.

3.4. Cyclic Potentiodynamic Polarization

Figure 5 shows the uncoated CPP for alloys and anodized samples in NaCl and H_2SO_4 at 3.5 wt. %. Figure 5a shows the behavior of Ti-6Al-2Sn-4Zr-2Mo uncoated and anodized when exposed to NaCl; the uncoated sample presents a higher E_{corr} when exposed to NaCl compared with the anodized sample of Ti-6Al-2Sn-4Zr-2Mo, -0.397 V (see Table 2), meaning that corrosion is most likely. The uncoated sample did not present a passivation zone, indicating activation and material dissolution. The sample anodized with H_2SO_4 showed the highest i_{corr} (4.53×10^{-7} A/cm²) in this media for the Ti-6Al-2Sn-4Zr-2Mo alloy; furthermore, the behavior corresponds to coating and means that the anodized sample presented a higher corrosion kinetics in comparison with the sample anodized in H_3PO_4 . The H_3PO_4 -anodized sample presented better corrosion resistance and did not show a significant passive breakdown potential, compared to that anodized in H_2SO_4 .

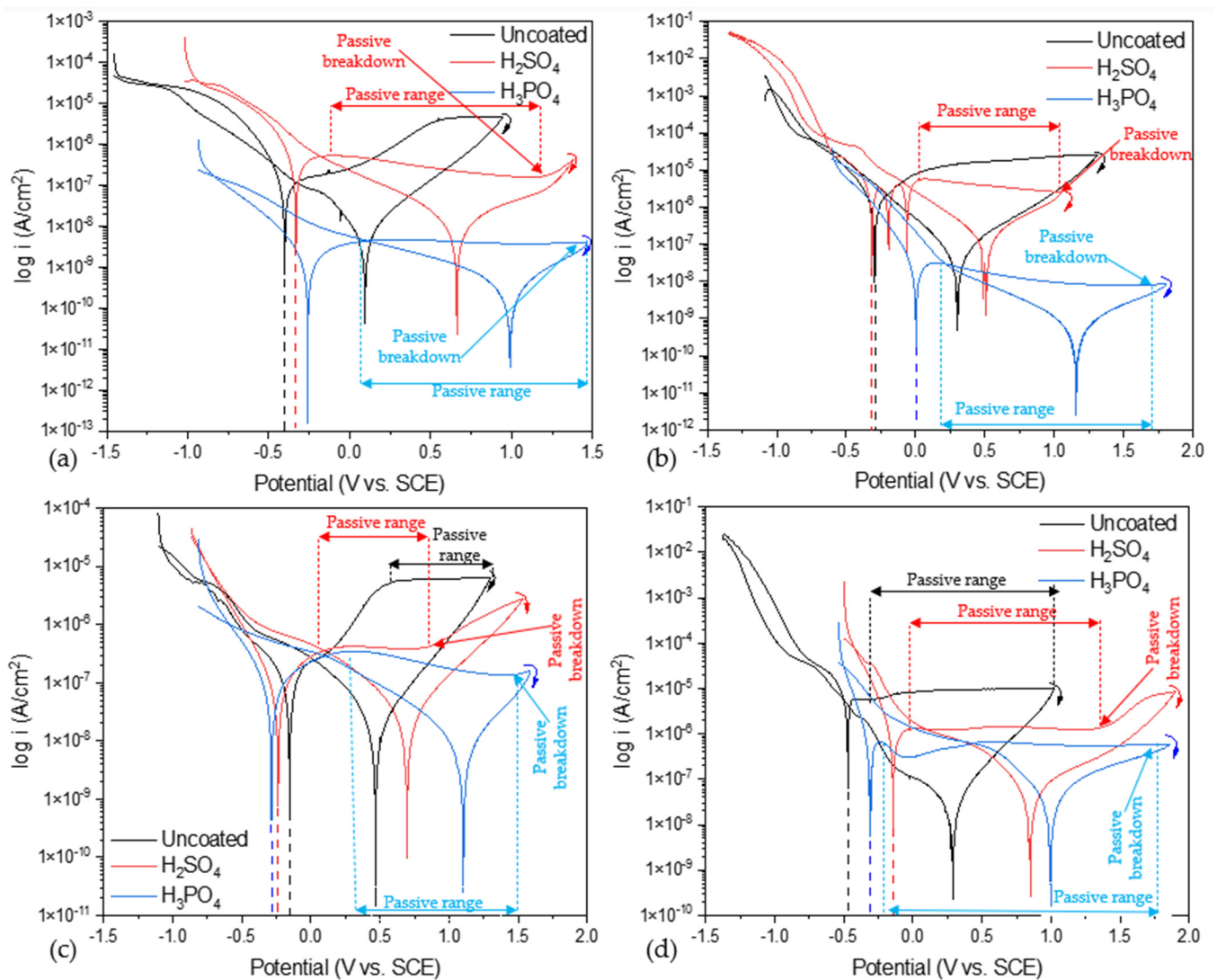


Figure 5. CPP of alloys and anodized samples (a) Ti-6Al-2Sn-4Zr-2Mo in NaCl, (b) Ti-6Al-2Sn-4Zr-2Mo in H₂SO₄, (c) Ti-6Al-4V in NaCl, and (d) Ti-6Al-4V in H₂SO₄.

Figure 5b shows the behavior of uncoated and anodized Ti-6Al-2Sn-4Zr-2Mo when exposed to H₂SO₄. In this case, the uncoated and the H₂SO₄-anodized sample presented similar values of E_{corr} (−0.301 and −0.312 V) and i_{corr} (1.86×10^{-6} and 4.23×10^{-6} A/cm²), meaning a similar corrosion probability and kinetics. However, the H₂SO₄-anodized sample presented three unusual reactions in the anodic branch, associated with a fast electrochemical reaction on the surface due to the porosity. Furthermore, that reaction in the anodic branch is related to an unstable oxide layer generated on the surface, and the pitting and repassivation process that occurs. Additionally, the sample anodized with H₂SO₄ presented a passivation range with a reduction of current demand, meaning that the corrosion process was reduced. The sample anodized with H₃PO₄ presented the highest E_{corr} in this media, −0.002 V, and lower i_{corr} , 3.24×10^{-8} A/cm², associated with a lower corrosion rate. The passivation range was more extended with 1.17 V, and a reduction of current was presented.

Table 2. Parameters obtained by CPP.

Sample	E_{corr} (V)	i_{corr} (A/cm ²)	Hysteresis	Range Passive (V)	Passive Breakdown (V)	Corrosion Rate (mpy)	$-\beta_c$ (V/decade)	β_a (V/decade)	β (v)	R_p ($\Omega \cdot \text{cm}^2$)
Ti-6Al-2Sn-4Zr-2Mo										
3.5 wt. % NaCl										
Uncoated	−0.397	1.0×10^{-7}	Negative	N/A	N/A	0.071	1.2×10^{-1}	7.1×10^{-1}	4.5×10^{-2}	4.2×10^5
H ₂ SO ₄	−0.330	4.5×10^{-7}	Negative	1.29	1.19	0.251	1.6×10^{-1}	1.4	6.2×10^{-2}	1.3×10^5
H ₃ PO ₄	−0.257	2.6×10^{-9}	Negative	1.24	1.42	0.0014	2.6×10^{-1}	7.8×10^{-1}	7.7×10^{-2}	2.9×10^7
3.5 wt. % H ₂ SO ₄										
Uncoated	−0.301	1.8×10^{-6}	Negative	N/A	N/A	1.39	2.4×10^{-1}	4.1×10^{-1}	6.7×10^{-2}	3.6×10^4
H ₂ SO ₄	−0.312	4.2×10^{-6}	Negative	0.96	1.02	5.85	3.1×10^{-1}	9.9×10^{-1}	1.0×10^{-1}	2.4×10^4
H ₃ PO ₄	−0.002	3.2×10^{-8}	Negative	1.24	1.42	0.022	1.8×10^{-1}	4.6×10^{-1}	5.6×10^{-2}	1.7×10^6
Ti-6Al-4V										
3.5 wt. % NaCl										
Uncoated	−0.144	1.0×10^{-7}	Negative	0.6552	1.28	0.0388	1.4×10^{-1}	1.5×10^{-1}	3.3×10^{-2}	3.2×10^5
H ₂ SO ₄	−0.237	1.2×10^{-7}	Negative	0.48	0.77	0.0848	3.2×10^{-1}	6.2×10^{-1}	9.3×10^{-2}	7.6×10^5
H ₃ PO ₄	−0.287	4.2×10^{-7}	Negative	1.17	1.44	0.1127	3.9×10^{-1}	1.8	1.3×10^{-1}	3.2×10^5
3.5 wt. % H ₂ SO ₄										
Uncoated	−0.475	6.7×10^{-6}	Negative	0.92	1.01	9.31	1.9×10^{-1}	11.2	8.3×10^{-2}	1.2×10^4
H ₂ SO ₄	−0.146	1.6×10^{-6}	Negative	1.27	1.28	0.991	1.3×10^{-1}	1.0	5.1×10^{-2}	3.1×10^4
H ₃ PO ₄	−0.318	4.6×10^{-7}	Negative	1.78	0.94	0.382	9.2×10^{-2}	6.9×10^{-1}	3.5×10^{-2}	7.7×10^4

Figure 5c shows the behavior of Ti-6Al-4V, uncoated and anodized, in NaCl at 3.5 wt %. The uncoated sample had the higher E_{corr} , −0.144 V (see Table 2) when exposed to NaCl and compared with the anodized of Ti-6Al-4V; meanwhile, the anodized sample in H₂SO₄ and H₃PO₄ presented −0.237 and −0.287 V (see Table 2). However, the uncoated sample presented the higher i_{corr} , with 6.71×10^{-6} , relating this behavior with a faster corrosion kinetic. All the samples presented passivation, the highest being for the sample anodized in H₃PO₄, meaning that the passive layer was more stable against corrosion processes. The sample anodized in H₃PO₄ presented a passive region of 1.28 V, and also presented a decrease in the current demand, from values near to $\times 10^{-6}$ to $\times 10^{-7}$ A/cm², meaning a reduction of electron transference, associated with an increase in the passive layer efficiency. The anodized sample of Ti-6Al-4V in H₂SO₄ presented a lower passivation range (0.77 V), but in that short period, the current demand remained uniform without increasing, relating the process with passivation.

The high porosity and low thickness of anodized H₂SO₄ are related to the faster passivity breakdown, shown in Figure 5c; that breakdown is of the passive layer generated in the corrosion process. The decrease in the current demand for the samples anodized in H₃PO₄ is related to the possible development of a passive layer in the anodized sample corresponding to a diffusion process.

Figure 5c shows the behavior of uncoated and anodized Ti-6Al-4V in H₂SO₄ at 3.5 wt %. The uncoated sample presented the lowest E_{corr} and highest i_{corr} (−0.475 V and 6.71×10^{-6} A/cm²) when exposed to H₂SO₄ media. For the anodized samples, the worst corrosion performance characterized by CPP was for H₂SO₄, which presented a higher i_{corr} (1.69×10^{-6} A/cm²) but presented a higher E_{corr} (−0.146 V), associating this behavior with the demand of energy to begin an anodic process. The passivation range was higher for anodized in H₃PO₄, giving rise to the best coating layer.

Table 2 shows the values of CPP obtained by Tafel interpolation and the range and passive breakdown. All the samples presented a negative hysteresis, meaning that the corrosion process occurring on the surface is uniform. The Ti-6Al-2Sn-4Zr-2Mo anodized in H₃PO₄ showed the best corrosion performances in both media with the lowest i_{corr} values

(2.64×10^{-9} and 3.24×10^{-8} A/cm²). Furthermore, the passivation zone did not present changes in current, which can be observed in the passivation range values.

In the case of Ti-6Al-2Sn-4Zr-2Mo, the sample anodized in H₃PO₄ showed the lowest corrosion rate in both media with 0.0014 and 0.022 mpy in NaCl and H₂SO₄. Even the polarization resistance was higher for the H₃PO₄ anodized sample, with values of 2.9×10^7 and 1.7×10^6 Ω·cm² for NaCl and H₂SO₄. In comparison with the sample anodized in H₂SO₄ and the uncoated sample, the one anodized in H₃PO₄ presented the best performance against corrosion.

For the Ti-6Al-4V, the sample anodized in H₂SO₄ presented a better corrosion performance in NaCl than the Ti-6Al-4V anodized in H₃PO₄ with corrosion rates of 0.0848 mpy. That performance was also higher than the Ti-6Al-2Sn-4Zr-2Mo anodized in H₂SO₄, meaning that samples anodized in H₂SO₄ showed a better conduct against corrosion when it was applied to Ti-6Al-4V. However, the R_p values presented showed a high dominance of the Ti-6Al-2Sn-4Zr-2Mo alloy in both anodized electrolytes, but it is important to consider the sample of Ti-6Al-4V anodized in H₂SO₄ as a good option for applications in acid media.

These results can be associated with a more uniform, compact, well-adherent oxide layer. However, samples anodized in H₃PO₄ had a higher porosity than those anodized in H₂SO₄. The former showed the best performance. The EIS technique may explain this phenomenon.

3.5. Electrochemical Impedance Spectroscopy

Figure 6a shows the Nyquist plot for anodized samples of Ti-6Al-2Sn-4Zr-2Mo exposed in NaCl at 3.5 wt. %. The uncoated sample presented titanium's typical behavior with the development of a natural passive layer. As shown in Figure 7a, the coated samples presented similar behavior when the process was governed by diffusion. The H₃PO₄ anodized samples presented a higher resistance to porosity (R_{por}) 5.42×10^4 Ω·cm². The porous layer is the first barrier, and afterward, the diffusion process occurs in the compact oxide layer, and the resistance increased for both samples.

In Figure 6b, the uncoated sample presented a different behavior compared to that presented in Figure 7b. This is related to the creation of a stable passive layer in H₂SO₄. The anodized samples showed processes dominated by diffusion. For those anodized in H₃PO₄, the Warburg's resistance increased, meaning that oxygen diffusion occurred, increasing the passive layer.

Figure 6c shows the behavior of Ti-6Al-4V in NaCl at 3.5 wt. %. The uncoated sample showed a higher resistance due to the resistance of the metal–electrolyte interface. The anodized porous layer was lower for the sample anodized in H₃PO₄. After the resistance of the porous layer, a diffusion process governed the system.

Figure 6d shows the behavior when Ti-6Al-4V and the anodized sample were exposed to H₂SO₄. The sample anodized in H₃PO₄ presented a higher value of Warburg's resistance, 9.16×10^5 A/cm². Such a behavior is related to creating a passive layer in the compact oxide barrier. The resistance of the porous layer was lower for this sample due to the high heterogeneous porosity. Furthermore, the Warburg's impedance increased as the thickness of the anodized samples was higher for H₃PO₄ than for H₂SO₄. This behavior was presented for NaCl. The porosity had the same conduct in NaCl and H₂SO₄.

Figure 7 shows the Bode diagrams; Figure 7a,b shows the Bode diagrams for impedance magnitude for Ti-6Al-2Sn-4Zr-2Mo. The samples anodized in H₃PO₄ presented the higher impedance resistance with values of $\times 10^6$ order; this can be related with a high corrosion resistance. For the samples of Ti-6Al-4V, Figure 7e shows that samples anodized in H₃PO₄ exposed to NaCl presented higher impedance, associated with higher corrosion resistance. On the other hand, when samples of Ti-6Al-4V were exposed to H₂SO₄ (Figure 7f) the impedance of the anodized sample decreased to $\times 10^5$ order; the values obtained were so close to the uncoated sample, that it meant a possible anodized dissolution.

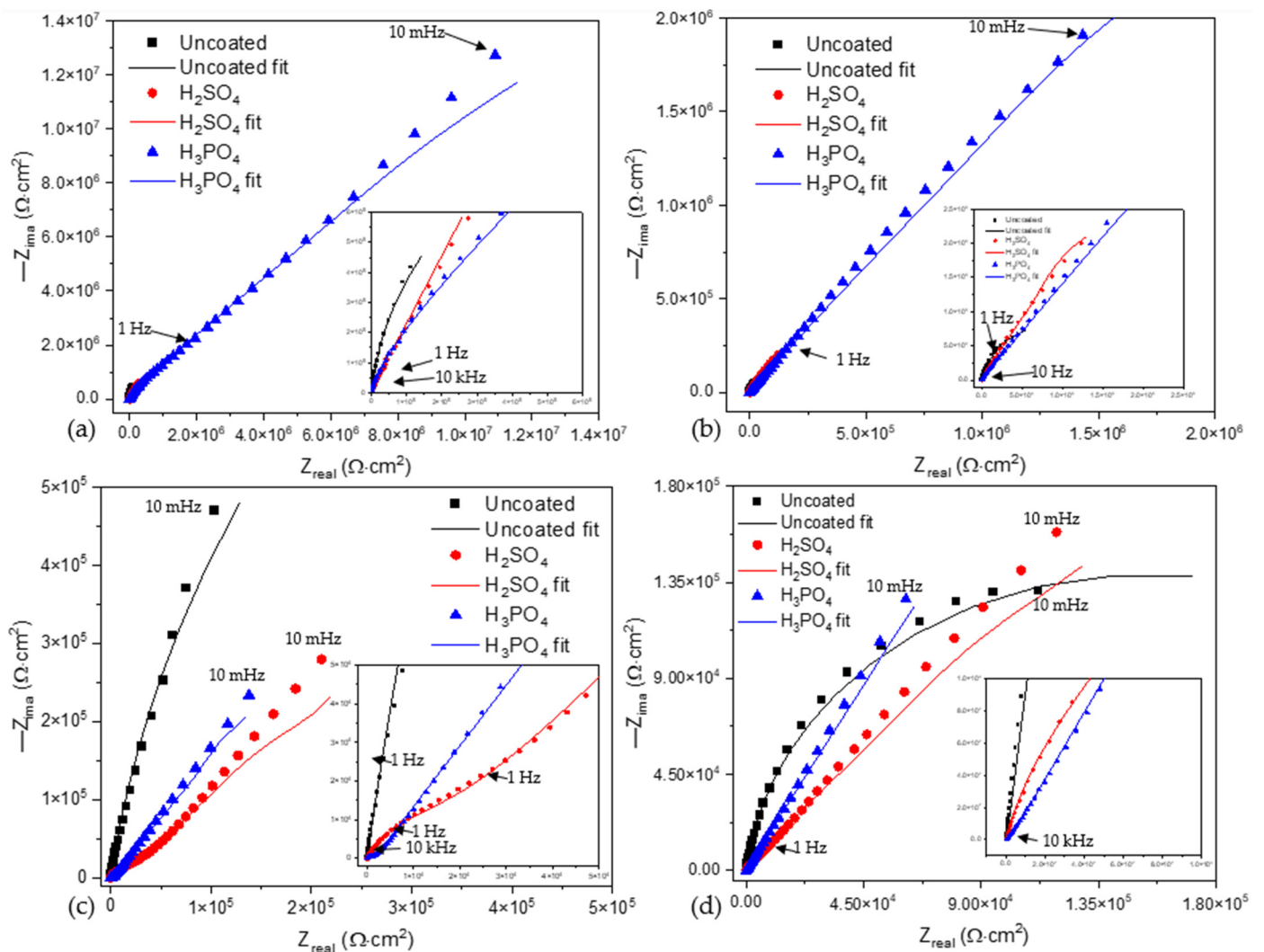


Figure 6. Nyquist plots of alloys and anodized samples (a) Ti-6Al-2Sn-4Zr-2Mo in NaCl, (b) Ti-6Al-2Sn-4Zr-2Mo in H₂SO₄, (c) Ti-6Al-4V in NaCl, and (d) Ti-6Al-4V in H₂SO₄.

Figure 7c,d show the Bode diagrams vs. angle phase; the uncoated sample showed one time constant in Figure 7c and two for Figure 7d. The anodized samples presented the superposition of signals, meaning that two processes were occurring at the same time; also, at low frequencies, a change in the slope was present. Figure 7g,d show Ti-6Al-4V; the uncoated sample presented the same behavior for one time constant. On the other hand, the anodized samples presented the behavior of two time constants, with a change in the process between 100 kHz and 1 Hz related to the behavior of intermetallic coatings. Both samples of Ti-6Al-4V showed the two time constants.

Figure 8 shows the equivalent circuit for the different systems. The uncoated samples present the typical R-CPE behavior of Figure 8a; only the Ti-6Al-2Sn-4Zr-2Mo sample presented the system from Figure 8b, related to the tendency to generate a passive layer in H₂SO₄, and the stability of this one. All the anodized samples showed an 8c circuit related to the resistance of the porosity barrier, and the diffusion in the compact barrier zone, associated with an increase in the barrier. Figure 9 shows the diffusion behavior of anodized samples, where the diffusion process begins in the barrier zone due to the compactness of the coating in that zone.

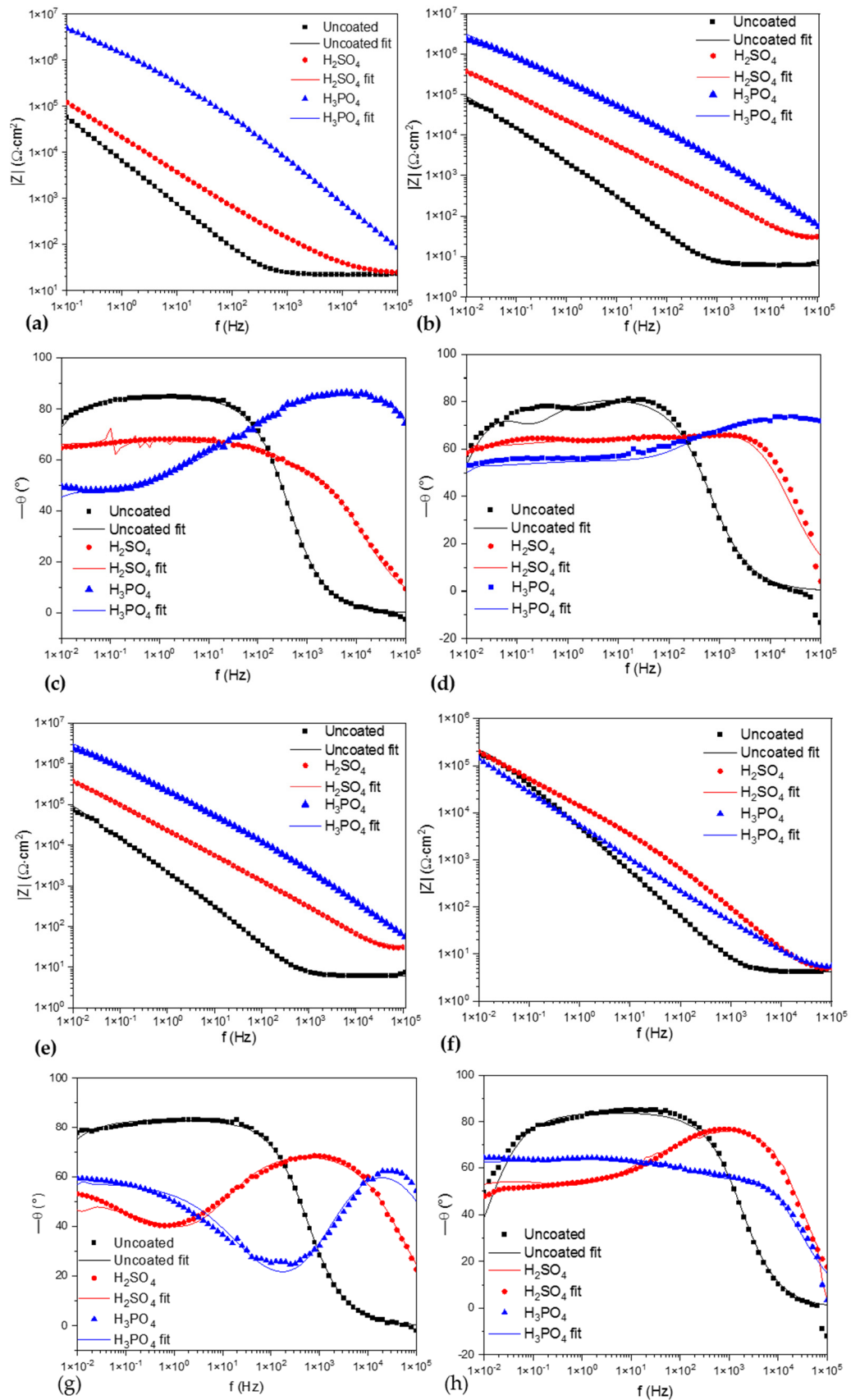


Figure 7. Bode vs. $|Z|$; (a) Ti-6Al-2Sn-4Zr-2Mo in NaCl, (b) Ti-6Al-2Sn-4Zr-2Mo in H_2SO_4 , (e) Ti-6Al-4V in NaCl, and (f) Ti-6Al-4V in H_2SO_4 . Bode diagrams vs. angle phase (θ°); (c) Ti-6Al-2Sn-4Zr-2Mo in NaCl, (d) Ti-6Al-2Sn-4Zr-2Mo in H_2SO_4 , (g) Ti-6Al-4V in NaCl, and (h) Ti-6Al-4V in H_2SO_4 .

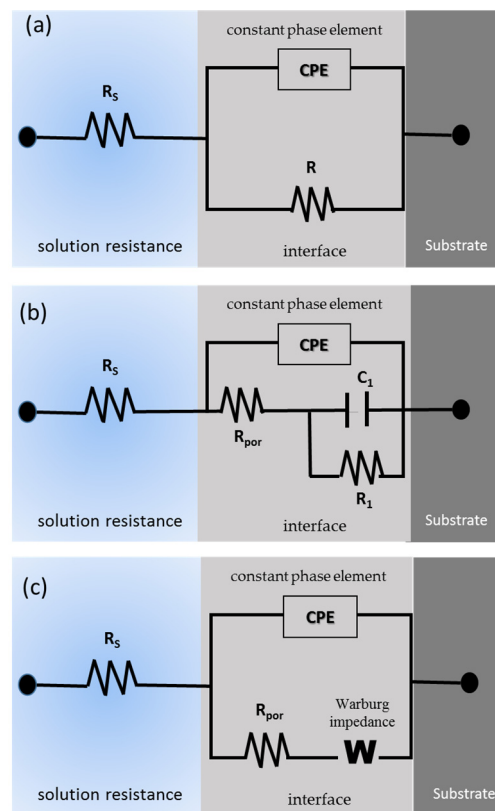


Figure 8. Equivalent circuit for (a) uncoated Ti-6Al-2Sn-4Zr-2Mo in NaCl and Ti-6Al-4V. (b) Ti-6Al-2Sn-4Zr-2Mo in H₂SO₄ and (c) for all the anodized samples.

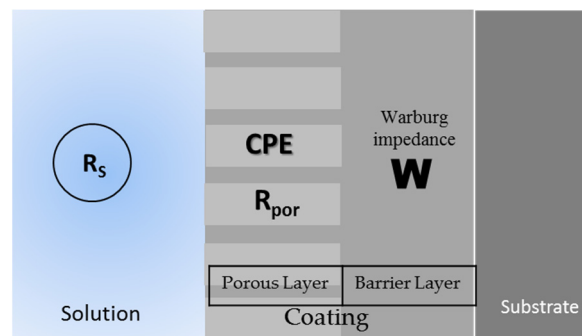


Figure 9. Corrosion system of the anodized samples.

Table 3 shows the parameters obtained by EIS. The anodized sample in Ti-6Al-2Sn-4Zr-2Mo presented lower capacitance values related to increased coating thickness. Furthermore, a porous barrier presented similar behavior. The samples anodized in H₂SO₄ showed lower values of n associated with a non-homogenous current distribution due to the heterogenous porosity of the samples, even Ti-6Al-2Sn-4Zr-2Mo and Ti-6Al-4V. The error of the equivalent circuit was acceptable for all the systems. The anodized Ti-6Al-2Sn-4Zr-2Mo presented this technique's best behavior against corrosion, with values of $\times 10^6$ and $\times 10^7$ A/cm². The order of the porous barrier was 10×4 A/cm², so the porosity was more homogenous and stable.

Table 3. Parameters obtained by EIS.

Sample	Rs ($\Omega \cdot \text{cm}^2$)	R _{por} ($\Omega \cdot \text{cm}^2$)	CPE (F/cm ²)	n	R ($\Omega \cdot \text{cm}^2$)	C ₁ (F/cm ²)	W ($\Omega \cdot \text{cm}^2$)	χ^2
Ti-6Al-2Sn-4Zr-2Mo								
3.5 wt. % NaCl								
Uncoated	21.9	2.23×10^6	2.75×10^{-5}	0.943	–	–	–	2.72×10^{-3}
H ₂ SO ₄	22.6	5.25×10^3	1.18×10^{-5}	0.737	–	–	7.80×10^6	9.90×10^{-4}
H ₃ PO ₄	18.7	5.42×10^4	2.75×10^{-5}	0.973	–	–	5.29×10^6	1.15×10^{-3}
3.5 wt. % H ₂ SO ₄								
Uncoated	6.09	2.57×10^4	8.81×10^{-5}	0.912	1.55×10^5	4.87×10^{-5}	–	1.19×10^{-2}
H ₂ SO ₄	3.96	2.83×10^2	7.28×10^{-6}	0.858	–	–	9.00×10^5	1.15×10^{-2}
H ₃ PO ₄	1.84	1.79×10^4	3.01×10^{-7}	0.824	–	–	1.01×10^7	4.46×10^{-3}
Ti-6Al-4V								
3.5 wt. % NaCl								
Uncoated	20.2	3.44×10^6	2.54×10^{-5}	0.925	–	–	–	2.24×10^{-3}
H ₂ SO ₄	20.8	2.42×10^4	2.26×10^{-5}	0.787	–	–	8.22×10^5	1.31×10^{-3}
H ₃ PO ₄	23.1	1.56×10^3	4.36×10^{-7}	0.802	–	–	7.16×10^5	5.09×10^{-3}
3.5 wt. % H ₂ SO ₄								
Uncoated	4.18	3.07×10^5	3.82×10^{-5}	0.935	–	–	–	2.11×10^{-2}
H ₂ SO ₄	4.35	2.17×10^3	3.97×10^{-6}	0.902	–	–	5.57×10^5	3.32×10^{-3}
H ₃ PO ₄	4.72	9.27×10^1	1.20×10^{-5}	0.822	–	–	9.16×10^5	1.65×10^{-3}

The following equation defines the calculation of the oxide film formed:

$$\delta_{\text{ox}} = \frac{\varepsilon \varepsilon_0}{C_{\text{cc}}}$$

In this case, the ε and ε_0 correspond to oxide film permittivity, and the vacuum permittivity ($8.85 \times 10^{-14} \text{ Fcm}^{-1}$) and C_{cc} are the system's capacitance. δ_{ox} is the thickness of the oxide film formed in the process. Table 4 shows the results of the thickness. The value of ε for TiO₂ was 86. The CPE can obtain the C_{cc} value from Table 3.

Table 4. Values of oxide film thickness generated by EIS.

Samples		δ (m)	
		3.5 wt. % NaCl	3.5 wt. % H ₂ SO ₄
Ti-6Al-2Sn-4Zr-2Mo	Uncoated	2.77×10^{-9}	8.62×10^{-11}
	H ₂ SO ₄	6.45×10^{-9}	1.05×10^{-8}
	H ₃ PO ₄	2.77×10^{-9}	2.53×10^{-7}
Ti-6Al-4V	Uncoated	2.15×10^{-9}	1.99×10^{-9}
	H ₂ SO ₄	3.37×10^{-9}	1.92×10^{-8}
	H ₃ PO ₄	1.75×10^{-7}	6.34×10^{-9}

The results of Table 4 show that the anodized samples of Ti-6Al-2Al-4Zr-2Mo presented high values for the oxide layer generated when anodized in H₃PO₄. For Ti-6Al-4V, the H₃PO₄ anodized samples showed a higher oxide generation in NaCl with 1.75×10^{-7} m than all the anodized Ti-6Al-4V in any media. It is important to mention that the anodization of Ti-6Al-2Sn-4Zr-2Mo presented an easier generation in H₂SO₄ and Ti-6Al-4V had easier growth in NaCl media. Figure 10 schematizes the process of oxide layer growth.

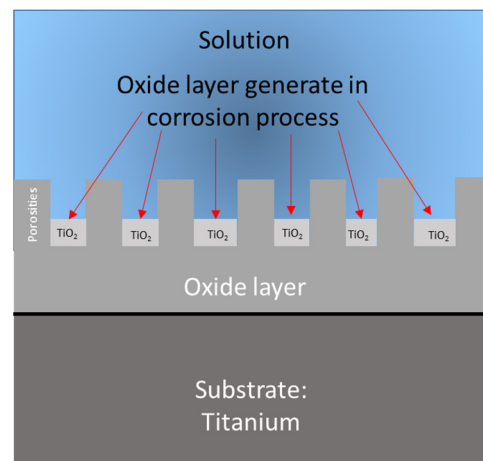


Figure 10. Schematization of oxide growth calculated by capacitance.

It is important to mention that the diffusion process begins in the oxide layer generated by the corrosion process due to the porosities of that part.

4. Discussion

Previous researchers have emphasized the role of the porosity of titanium alloys concerning their mechanical and corrosion resistance. Both samples showed porosity in both samples, decreasing the mechanical and corrosion resistance due to the pores being stress concentrators. This, in turn, makes the material susceptible to localized corrosion. However, the material can repassivate it. The tiny pores help to reduce the diffusion process in the electrolytes [49,50]. In this case, Ti-6Al-2Sn-4Zr-2Mo had a higher porosity, but the size was smaller than in Ti-6Al-4V and localized in β phases [51,52].

In Figure 1b, the microstructure of Ti-6Al-4V and the porosity can make the material vulnerable to problems in the coating. Kumar [53] mentioned that H_2SO_4 , an anodized electrolyte, produces a stable oxide layer. For that reason, the thickness of the anodized samples in H_2SO_4 presented less variation in thickness measurements since the concentration of 1M helped the correct flow of current.

The reaction in the anodic breach of Ti-6Al-2Sn-4Zr-2Mo anodized in H_2SO_4 was explained by Cabral et al. [54] as a cathodic–anodic behavior in the system; however, various authors related the reaction to the change in the electrolyte concentration when there was a variation in pH and oxide reduction. Furthermore, it can be associated with a reduction of the protective layer [55–59]. For this anodized sample, the behavior presented was related to the reduction of anodized protection caused by oxygen reduction, and OH^- ions attacking the surface because of the heterogenous nature of the anodized sample. The continuity of the other passivation zones is related to forming an oxide film in the passivated or anodized surface [60,61].

However, the high thickness of the sample anodized in H_3PO_4 is associated with continuous oxygen evolution; when it occurs in the anodizing process, it increases the thickness, and it is also reported by various authors [62–66]. Conversely, El-Taib Heakal et al. [67] mentioned that anodized H_3PO_4 presented better behavior against dissolution than H_2SO_4 . However, this research showed that anodizing in H_3PO_4 presented better behavior against dissolution by using CPP and EIS. It can be observed in the anodic breach of CPP, where the current densities of the passive layer in H_2SO_4 presented high current demand in the system. The breaking potential of the passive layer is also lower than samples anodized in H_3PO_4 , indicating higher anodized stability. The facility of the diffusion process corresponds to the electrolyte resistance, and the low ionic resistance describes a faster kinetic [68].

Martinez et al. [69] related the increase in current density (i_{CORR}) to a passive layer that does not contribute to corrosion protection, and also associated the increase in current

density of passivation with an oxygen and chlorine evolution. Furthermore, they correlated the incorporation of Mo to inhibit chloride ion absorption. For that reason, the increase in corrosion resistance calculated by CPP was higher for Ti-6Al-2Sn-4Zr-2Mo, decreasing the dissolution.

The low corrosion rate of Ti-6Al-2Sn-4Zr-2Mo anodized in H₃PO₄ (0.0014 and 0.022 mpy) is related to lower anodized dissolution and the generation of a layer generated by the corrosion process. The EIS characterization can corroborate that behavior.

The EIS double circle shown in Figure 6b, for the uncoated Ti-6Al-2Sn-4Zr-2Mo at low frequencies, is related to the layer of the corrosion products and is called the double electrochemical layer [70]. The value of “n” has different interpretations depending on the authors. Fouda et al. [71] related the value of 1 with an ideal capacitor, and reducing values reduces the charge of samples. Gomes et al. [72] related the CPE behavior with the resistivity distribution in the thin oxide layer thickness. This method is possible and easily determines the oxide thickness. The second time constant is related to the diffusion inside the oxide layer. For that reason, Gateman et al. [73] concluded that CPE was directly related to the interfacial properties of the system, and the correct analysis would depend directly on that. Meanwhile, the n value being near 1 is related to a more homogenous surface. Furthermore, the values are related to capacitive systems, where energy accumulation begins with the process of charge transference.

The physical meaning of CPE has been a discussion motif for diverse authors. Macdonald et al. [74–76] mentioned that CPE represents the conductive behavior of the dielectric; however, the modeling is complex, and it is not easy to give an exactitude of the nature of the system. On the other hand, authors relate the CPE with the phenomenon of surface roughness, and when “n” values are between 1 and 0.9, the system is dominated by a power law; meanwhile, when the value is 0.5, there is talk of a contorted surface (Warburg’s diffusion) [77]. Kim et al. [78] related the CPE with the homogeneity of the surface reactions, and once Schiller et al. [79] associated CPE with the thickness composition and variation. Córdoba-Torres [80] mentioned that CPE at high frequencies is related to a less resistive film (in zones) and, at low frequencies, is associated with the power law distribution, dominating the low resistivity behavior of the distribution function. In this work, the results of CPE are directly related to the surface’s homogeneity and resistance; when the “n” value was near 1, the coating presented better properties against corrosion.

Additionally, that behavior can be observed in EIS with the increase in diffusion resistance represented by Warburg’s element (W), meaning that the oxide layer is more stable and increased.

Some authors relate the Warburg impedance at low frequencies with redox molecules that diffuse in the system, giving a high Warburg impedance. However, when the Warburg process occurs at high frequencies, it is associated with low impedance values [81]. In this case, the high values of the Warburg resistance were consequent to a diffusion process that occurred in the compact oxide layer–electrolyte interface, increasing the resistance of the anodized samples. Rajan et al. [82] associated the disappearance in the coating of Warburg impedance with the inhibition of diffusion, so the coating layer is very protective. It is essential to mention that the electrochemical reaction governed by the Warburg impedance is absorption, penetration and diffusion [83]. The absorption–penetration occurs in the porous zone and the interface of the compact barrier and the diffusion in the compact barrier; that process produces an increase in the properties against corrosion.

The process that decreases the corrosion rate by diffusion occurs with the continuous development of a passive layer by the following reaction [84]:



For the electrolytes that contain Cl[−] ions, the colocation of the ions in titanium or the anodized surface to form titanium oxide actuates by the following reactions:





These results show that the diffusion process in titanium and titanium anodized surfaces occurs on the solid phase due to the diffusion of metal ions in the porous layer. The micropores of the first oxide layer act as preferent diffusion sites for the solution ions [85–89].

The use of the constant phase element in the equivalent circuits is related to the non-ideal behavior of the capacitor. The physical explanation of this phenomenon is that the surface is non-homogeneous and presents porosities or differences in roughness [86,88]. Therefore, the value of “n” in the CPE element is lower for anodized H_2SO_4 . The imperfection in the anodized sample is higher; meanwhile, in H_3PO_4 , the values of “n” are close to 1, so the surface is more homogenous. Anodized Ti-6Al-4V presented values of “n” related to heterogeneities in the surface.

Sadek et al. [90] mentioned that the formation of a hydroxide layer ($\text{Ti}(\text{OH})_x\text{O}_y$) is due to a limitation in the oxidation process by the increase in oxide. The layer created by the hydroxide is porous, resulting in diffusion [91–93]. This behavior is observed in Figure 5b of CPP, where a fast reaction produced the reaction in the anodic branch. In EIS, the effects of hydroxide and secondary oxides are associated with the graphics of the capacitive response [36].

5. Conclusions

- The anodized Ti-6Al-2Sn-4Zr-2Mo alloys presented the best properties against corrosion, as analyzed by the electrochemical techniques employed in this research work. This behavior is related to Mo and Zr presence in the alloy and the anodized forms.
- The anodizing H_2SO_4 solution showed a smaller porosity than the H_3PO_4 anodizing solution. However, the lower porosity helped to prevent ion penetration by capillarity.
- The samples of both alloys anodized in H_3PO_4 presented the biggest thickness measurement by SEM of the anodization with a maximum value of 2.08 μm . The presence of oxygen was higher in the oxide layer.
- The sample of Ti-6Al-2Sn-4Zr-2Mo presented the highest oxide growth of all, at 2.53×10^{-7} m, when it was anodized in H_3PO_4 and exposed to H_2SO_4 . Meanwhile, the Ti-6Al-4V presented the lowest oxide growth layer (3.57×10^{-9} m).
- The H_2SO_4 -anodized sample for Ti-6Al-4V did not reach the minimum specifications to accomplish the thickness required for AMS2487B for anodized aeronautical titanium. Furthermore, both Ti-6Al-4V anodized samples presented the imperfections of high roughness and lack of adherence.
- For characterization of the CPP, the alloys anodized with H_3PO_4 presented lower i_{corr} , meaning a lower corrosion kinetic. Additionally, both H_2SO_4 -anodized samples exposed to NaCl presented current densities similar to uncoated samples, meaning that the Cl^- could easily penetrate the anodizing layer.
- The samples of Ti-6Al-4V presented high corrosion rate values (between 0.084 and 0.991 mpy); meanwhile, Ti-6Al-2Sn-4Zr-2Mo showed the lowest corrosion rate values of all the systems in NaCl and H_2SO_4 (0.0014 and 0.022 mpy).
- All the anodized samples studied by EIS were governed by a diffusion process represented by the Warburg element. The diffusion occurred after the porous layer finished in the compact oxide layer of anodization, meaning that the anodization protects the titanium from the electrolyte.
- The results obtained by CPP and EIS converged to characterize the anodized samples, where the results showed that Ti-6Al-2Sn-4Zr-2Mo anodized in H_3PO_4 presented the best properties against corrosion from both techniques. Furthermore, the results matched with the SEM characterization where the anodized samples presented the higher thickness (1.62 μm on average).

Author Contributions: Conceptualization, J.M.J.-M., F.A.-C. and C.G.-T.; methodology, J.M.J.-M., F.E.-L., J.C.-R. and J.P.F.-D.I.R.; data curation, F.E.-L., C.T.M.-R., F.A.-C. and J.M.J.-M.; formal analysis,

J.M.J.-M., F.A.-C., M.Á.B.-Z., R.G.B.-M. and C.G.-T.; writing—review and editing, J.M.J.-M., F.A.-C. and C.G.-T. All authors have read and agreed to the published version of the manuscript.

Funding: This research was funded by the Mexican National Council for Science and Technology (CONACYT) and the Universidad Autónoma de Nuevo León (UANL).

Data Availability Statement: Not applicable.

Acknowledgments: The authors acknowledge the Academic Body UANL—CA-316 “Deterioration and integrity of composite materials”.

Conflicts of Interest: The authors declare no conflict of interest.

References

1. Oliveira, V.M.C.A.; Aguiar, C.; Vazquez, A.M.; Robin, A.; Barboza, M.J.R. Improving Corrosion Resistance of Ti-6Al-4V Alloy through Plasma-Assisted PVD Deposited Nitride Coatings. *Corros. Sci.* **2014**, *88*, 317–327. [[CrossRef](#)]
2. Diamanti, M.V.; Pedferri, M.P. Effect of Anodic Oxidation Parameters on the Titanium Oxides Formation. *Corros. Sci.* **2007**, *49*, 939–948. [[CrossRef](#)]
3. Minagar, S.; Wang, J.; Berndt, C.C.; Ivanova, E.P.; Wen, C. Cell Response of Anodized Nanotubes on Titanium and Titanium Alloys. *J. Biomed. Mater. Res. Part A* **2013**, *101*, 2726–2739. [[CrossRef](#)] [[PubMed](#)]
4. Hanawa, T. Metal Ion Release from Metal Implants. *Mater. Sci. Eng. C* **2004**, *24*, 745–752. [[CrossRef](#)]
5. Jiang, Z.; Norby, T.; Middleton, H. Evaluation of Metastable Pitting on Titanium by Charge Integration of Current Transients. *Corros. Sci.* **2010**, *52*, 3158–3161. [[CrossRef](#)]
6. Li, S.; Yao, W.; Liu, J.; Yu, M.; Wu, L.; Ma, K. Study on Anodic Oxidation Process and Property of Composite Film Formed on Ti-10V-2Fe-3Al Alloy in SiC Nanoparticle Suspension. *Surf. Coatings Technol.* **2015**, *277*, 234–241. [[CrossRef](#)]
7. Peters, M.; Kumpfert, J.; Ward, C.H.; Leyens, C. Titanium Alloys for Aerospace Applications. *Adv. Eng. Mater.* **2003**, *5*, 419–427. [[CrossRef](#)]
8. Gloria, A.; Montanari, R.; Richetta, M.; Varone, A. Alloys for Aeronautic Applications: State of the Art and Perspectives. *Metals* **2019**, *9*, 662. [[CrossRef](#)]
9. Song, H.J.; Kim, M.K.; Jung, G.C.; Vang, M.S.; Park, Y.J. The Effects of Spark Anodizing Treatment of Pure Titanium Metals and Titanium Alloys on Corrosion Characteristics. *Surf. Coat. Technol.* **2007**, *201*, 8738–8745. [[CrossRef](#)]
10. Kim, H.Y.; Miyazaki, S. Martensitic Transformation and Superelastic Properties of Ti-Nb Base Alloys. *Mater. Trans.* **2015**, *56*, 625–634. [[CrossRef](#)]
11. Martínez, C.; Guerra, C.; Silva, D.; Cubillos, M.; Briones, F.; Muñoz, L.; Páez, M.A.; Aguilar, C.; Sancy, M. Effect of Porosity on Mechanical and Electrochemical Properties of Ti-6Al-4V Alloy. *Electrochim. Acta* **2020**, *338*, 135858. [[CrossRef](#)]
12. Castany, P.; Gordin, D.M.; Drob, S.I.; Vasilescu, C.; Mitran, V.; Cimpean, A.; Gloriant, T. Deformation Mechanisms and Biocompatibility of the Superelastic Ti-23Nb-0.7Ta-2Zr-0.5N alloy. *Shape Mem. Superelasticity* **2016**, *2*, 18–28. [[CrossRef](#)]
13. Almeraya-Calderón, F.; Jáquez-Muñoz, J.M.; Lara-Banda, M.; Zambrano-Robledo, P.; Cabral-Miramontes, J.A.; Lira-Martínez, A.; Estupinán-López, F.; Tiburcio, C.G. Corrosion Behavior of Titanium and Titanium Alloys in Ringer’s Solution. *Int. J. Electrochem. Sci.* **2022**, *17*. [[CrossRef](#)]
14. Martínez-Villafaña, A.; Almeraya-Calderón, M.F.; Gaona-Tiburcio, C.; Gonzalez-Rodriguez, J.G.; Porcayo-Calderón, J. High-Temperature Degradation and Protection of Ferritic and Austenitic Steels in Steam Generators. *J. Mater. Eng. Perform.* **1997**, *7*, 108–113. [[CrossRef](#)]
15. Loch, J.; Łukaszczyk, A.; Vignal, V.; Krawiec, H. Corrosion Behaviour of Ti6Al4V and TiMo10Zr4 Alloys in the Ringer’s Solution: Effect of PH and Plastic Strain. *Solid State Phenom.* **2015**, *227*, 435–438. [[CrossRef](#)]
16. Khulief, Z.T.; Abdulameer, M. Corrosion Behavior of Different Types Titanium Alloys for Biomedical Applications. *AIP Conf. Proc.* **2022**, *2450*, 020023. [[CrossRef](#)]
17. Xu, Y.F.; Xiao, Y.F.; Yi, D.Q.; Liu, H.Q.; Wu, L.; Wen, J. Corrosion Behavior of Ti-Nb-Ta-Zr-Fe Alloy for Biomedical Applications in Ringer’s Solution. *Trans. Nonferrous Met. Soc. China* **2015**, *25*, 2556–2563. [[CrossRef](#)]
18. Rao, B.M.; Torabi, A.; Varghese, O.K. Anodically Grown Functional Oxide Nanotubes and Applications. *MRS Commun.* **2016**, *6*, 375–396. [[CrossRef](#)]
19. Sul, Y.T.; Johansson, C.B.; Petronis, S.; Krozer, A.; Jeong, Y.; Wennerberg, A.; Albrektsson, T. Characteristics of the Surface Oxides on Turned and Electrochemically Oxidized Pure Titanium Implants up to Dielectric Breakdown: The Oxide Thickness, Micropore Configurations, Surface Roughness, Crystal Structure and Chemical Composition. *Biomaterials* **2002**, *23*, 491–501. [[CrossRef](#)]
20. Wang, Z.B.; Hu, H.X.; Zheng, Y.G. Synergistic Effects of Fluoride and Chloride on General Corrosion Behavior of AISI 316 Stainless Steel and Pure Titanium in H₂SO₄ Solutions. *Corros. Sci.* **2018**, *130*, 203–217. [[CrossRef](#)]
21. Alam, M.J.; Cameron, D.C. Preparation and Characterization of TiO₂ Thin Films by Sol-Gel Method. *J. Sol-Gel Sci. Technol.* **2002**, *25*, 137–145. [[CrossRef](#)]
22. Diamanti, M.V.; Codeluppi, S.; Cordioli, A.; Pedferri, M.P. Effect of Thermal Oxidation on Titanium Oxides’ Characteristics. *J. Exp. Nanosci.* **2009**, *4*, 365–372. [[CrossRef](#)]

23. Löbl, P.; Huppertz, M.; Mergel, D. Nucleation and Growth in TiO₂ Films Prepared by Sputtering and Evaporation. *Thin Solid Films* **1994**, *251*, 72–79. [[CrossRef](#)]
24. Zhang, L.; Duan, Y.; Gao, R.; Yang, J.; Wei, K.; Tang, D.; Fu, T. The Effect of Potential on Surface Characteristic and Corrosion Resistance of Anodic Oxide Film Formed on Commercial Pure Titanium at the Potentiodynamic-Aging Mode. *Materials* **2019**, *12*, 370. [[CrossRef](#)] [[PubMed](#)]
25. Narayanan, R.; Seshadri, S.K. Phosphoric Acid Anodization of Ti–6Al–4V—Structural and Corrosion Aspects. *Corros. Sci.* **2007**, *49*, 542–558. [[CrossRef](#)]
26. Jáquez-Muñoz, J.M.; Gaona-Tiburcio, C.; Chacón-Nava, J.; Cabral-Miramontes, J.; Nieves-Mendoza, D.; Maldonado-Bandala, E.M.; Delgado, A.D.; Flores-De Los Rios, J.P.; Bocchetta, P.; Almeraya-Calderón, F. Electrochemical Corrosion of Titanium and Titanium Alloys Anodized in H₂SO₄ and H₃PO₄ Solutions. *Coatings* **2022**, *12*, 325. [[CrossRef](#)]
27. Jáquez-Muñoz, J.M.; Gaona-Tiburcio, C.; Cabral-Miramontes, J.; Nieves-Mendoza, D.; Maldonado-Bandala, E.; Olgún-Coca, J.; López-Léon, L.D.; De Los Rios, J.P.F.; Almeraya-Calderón, F. Electrochemical Noise Analysis of the Corrosion of Titanium Alloys in NaCl and H₂SO₄ Solutions. *Metals* **2021**, *11*, 105. [[CrossRef](#)]
28. Gaona-Tiburcio, C.; Montoya, R.M.; Cabral, M.J.A.; Estupiñán, L.F.; Zambrano, R.P.; Orozco, C.R.; Chacon-Nava, J.G.; Baltazar, Z.M.A.; Almeraya-Calderon, F. Corrosion resistance of multilayer coatings deposited by PVD on inconel 718 using electrochemical impedance spectroscopy technique. *Coatings* **2020**, *10*, 521. [[CrossRef](#)]
29. Jáquez-Munöz, J.M.; Gaona-Tiburcio, C.; Cabral, J.A.; Lara-Banda, M.; Estupiñán-López, F.H.; Zambrano, P.R.; Almeraya-Calderón, F. Corrosion Behaviour of Titanium Alloys Using Electrochemical Noise. *ECS Trans.* **2021**, *101*, 1.
30. Samaniego-Gámez, O.; Almeraya-Calderón, F.; Chacón-Nava, J.; Maldonado-Bandala, E.; Nieves-Mendoza, D.; Flores-De los Rios, J.P.; Jáquez-Muñoz, J.M.; Delgado, A.D.; Gaona-Tiburcio, C. Corrosion Behavior of Passivated CUSTOM450 and AM350 Stainless Steels For Aeronautical Applications. *Metals* **2022**, *12*, 666. [[CrossRef](#)]
31. Jaroenworoluck, A.; Regonini, D.; Bowen, C.R.; Stevens, R.; Allsopp, D. Macro, Micro and Nanostructure of TiO₂ Anodised Films Prepared in a Fluorine-Containing Electrolyte. *J. Mater. Sci.* **2007**, *42*, 6729–6734. [[CrossRef](#)]
32. Regonini, D.; Bowen, C.R.; Jaroenworoluck, A.; Stevens, R. A Review of Growth Mechanism, Structure and Crystallinity of Anodized TiO₂ Nanotubes. *Mater. Sci. Eng. R Rep.* **2013**, *74*, 377–406. [[CrossRef](#)]
33. Diaz, E.F.; Gonzalez-Rodriguez, J.G.; Martinez-Villafañe, A.; Gaona-Tiburcio, C. H₂S Corrosion Inhibition of an Ultra High Strength Pipeline by Carboxyethyl-Imidazoline. *J. Appl. Electrochem.* **2010**, *40*, 1633–1640. [[CrossRef](#)]
34. Samaniego-Gámez, P.; Almeraya-Calderón, F.; Martin, U.; Ressa, J.; Gaona-Tiburcio, C.; Silva-Vidaurri, L.; Ca-bral-Miramontes, J.; Bastidas, J.M.; Chacón-Nava, J.G.; Bastidas, D.M. Efecto del tratamiento de sellado en el comporta-miento frente a corrosión de la aleación anodizada de aluminio-litio AA2099. *Rev. Metal.* **2020**, *56*, e180. [[CrossRef](#)]
35. Socorro-Perdomo, P.P.; Florido-Suárez, N.R.; Mirza-Rosca, J.C.; Saceleanu, M.V. EIS Characterization of Ti Alloys in Relation to Alloying Additions of Ta. *Materials* **2022**, *15*, 476. [[CrossRef](#)]
36. Chávez-Díaz, M.P.; Luna-Sánchez, R.M.; Vazquez-Arenas, J.; Lartundo-Rojas, L.; Hallen, J.M.; Cabrera-Sierra, R. XPS and EIS Studies to Account for the Passive Behavior of the Alloy Ti-6Al-4V in Hank's Solution. *J. Solid State Electrochem.* **2019**, *23*, 3187–3196. [[CrossRef](#)]
37. Feizi Mohazzab, B.; Jaleh, B.; Kakuee, O.; Fattah-alhosseini, A. Formation of Titanium Carbide on the Titanium Surface Using Laser Ablation in N-Heptane and Investigating Its Corrosion Resistance. *Appl. Surf. Sci.* **2019**, *478*, 623–635. [[CrossRef](#)]
38. Ibriş, N.; Mirza Rosca, J.C. EIS Study of Ti and Its Alloys in Biological Media. *J. Electroanal. Chem.* **2002**, *526*, 53–62. [[CrossRef](#)]
39. Fakhr Nabavi, H.; Aliofkhaezrai, M. Morphology, Composition and Electrochemical Properties of Bioactive-TiO₂/HA on CP-Ti and Ti6Al4V Substrates Fabricated by Alkali Treatment of Hybrid Plasma Electrolytic Oxidation Process (Estimation of Porosity from EIS Results). *Surf. Coat. Technol.* **2019**, *375*, 266–291. [[CrossRef](#)]
40. Liu, C.; Bi, Q.; Leyland, A.; Matthews, A. An Electrochemical Impedance Spectroscopy Study of the Corrosion Behaviour of PVD Coated Steels in 0.5 N NaCl Aqueous Solution: Part II.: EIS Interpretation of Corrosion Behaviour. *Corros. Sci.* **2003**, *45*, 1257–1273. [[CrossRef](#)]
41. Kulova, T.; Gryzlov, D.; Skundin, A.; Gavrilin, I.; Martynova, I.; Kudryashova, Y. Causes of Germanium Phosphide Degradation under Prolonged Cycling. EIS Study. *Int. J. Electrochem. Sci.* **2022**, *17*, 220224. [[CrossRef](#)]
42. Deng, C.; Zhao, Z.; Hu, H.; Li, X.; Luo, W. Comparisons of I- and Cl- Concentrations on the Corrosion Behavior of TA4 Titanium Alloy in Azeotropic Acetic Acid Solutions. *J. Phys. Conf. Ser.* **2022**, *2368*, 012009. [[CrossRef](#)]
43. ASTM E3-95; Standard Practice for Preparation of Metallographic Specimens. ASTM International: West Conshohocken, PA, USA, 1995.
44. ASTM E407-07; Standard Practice for Microetching Metals and Alloys. ASTM International: West Conshohocken, PA, USA, 2011.
45. AMS2487; Anodic Treatment of Titanium and Titanium Alloys Solution pH 12.4 Maximum. SAE International: Warrendale, PA, USA, 2018.
46. ASTM G5-14; Standard Reference Test Method for Making Potentiodynamic Anodic Polarization. ASTM International: West Conshohocken, PA, USA, 2014.
47. ASTM G61-86; Standards Test Method for Conducting Cyclic Potentiodynamic Polarization Measurements for Localized Corrosion Susceptibility of Iron-, Nickel-, or Cobalt-Based Alloys. ASTM International: West Conshohocken, PA, USA, 2018.
48. ASTM G106-15; Standard Practice for Verification of Algorithm and Equipment for Electrochemical Impedance Measurements. ASTM International: West Conshohocken, PA, USA, 2015.

49. Sam Froes, F.H.; Qian, M.; Niinomi, M. An Introduction to Titanium in Consumer Applications. In *Titanium for Consumer Applications—Real World Use of Titanium*; Elsevier: Amsterdam, The Netherlands, 2019; pp. 1–12. [[CrossRef](#)]
50. Pałka, K.; Pokrowiecki, R.; Krzywicka, M. Porous Titanium Materials and Applications. In *Titanium for Consumer Applications—Real World Use of Titanium*; Elsevier: Amsterdam, The Netherlands, 2019; pp. 27–75. [[CrossRef](#)]
51. Esmailzadeh, S.; Aliofkhaezai, M.; Sarlak, H. Interpretation of Cyclic Potentiodynamic Polarization Test Results for Study of Corrosion Behavior of Metals: A Review. *Prot. Met. Phys. Chem. Surf.* **2018**, *54*, 976–989. [[CrossRef](#)]
52. Santiago, G.; Baltazar, M.A.; Galván, R.; López, L.; Zapata, F.; Zambrano, P.; Gaona, C.; Almeraya, F. Electrochemical Evaluation of Reinforcement Concrete Exposed to Soil Type SP Contaminated with Sulphates. *Int. J. Electrochem. Sci.* **2016**, *11*, 4850–4864. [[CrossRef](#)]
53. Kumar, A. Anodization of Titanium Alloy (Grade 5) to Obtain Nanoporous Surface Using Sulfuric Acid Electrolyte. *IETE J. Res.* **2022**, *68*, 3855–3861. [[CrossRef](#)]
54. Cabral Miramontes, J.A.; Barceinas Sánchez, J.D.O.; Almeraya Calderón, F.; Martínez Villafañe, A.; Chacón Nava, J.G. Effect of Boron Additions on Sintering and Densification of a Ferritic Stainless Steel. *J. Mater. Eng. Perform.* **2010**, *19*, 880–884. [[CrossRef](#)]
55. Jaquez-Muñoz, J.; Gaona-Tiburcio, C.; Lira-Martinez, A.; Zambrano-Robledo, P.; Maldonado-Bandala, E.; Samaniego-Gamez, O.; Nieves-Mendoza, D.; Olguin-Coca, J.; Estupiñan-Lopez, F.; Almeraya-Calderon, F. Susceptibility to Pitting Corrosion of Ti-CP2, Ti-6Al-2Sn-4Zr-2Mo, and Ti-6Al-4V Alloys for Aeronautical Applications. *Metals* **2021**, *11*, 1002. [[CrossRef](#)]
56. Maldonado-Bandala, E.; Jiménez-Quero, V.; Olguin-Coca, J.; Lizarraga, L.G.; Baltazar-Zamora, M.A.; Ortiz, A.; Almeraya, C.F.; Zambrano, R.P.; Gaona-Tiburcio, C. Electrochemical Characterization of Modified Concretes with Sugar Cane Bagasse Ash. *Int. J. Electrochem. Sci.* **2011**, *6*, 4915–4926.
57. Beavers, J.A.; Durr, C.L.; Thompson, N.G. Unique Interpretations of Potentiodynamic Polarization Technique. In Proceedings of the NACE—International Corrosion Conference Series, San Diego, CA, USA, 22–27 March 1998; Volume 1998.
58. Cabral-Miramontes, J.A.; Bastidas, D.M.; Baltazar, M.A.; Zambrano-Robledo, P.; Bastidas, J.M.; Almeraya-Calderón, F.M.; Gaona-Tiburcio, C. Corrosion Behavior of Zn-TiO₂ and Zn-ZnO Electrodeposited Coatings in 3.5% NaCl Solution. *Int. J. Electrochem. Sci.* **2019**, *14*, 4226–4239. [[CrossRef](#)]
59. Ramgopal, T.; Schmutz, P.; Frankel, G.S. Electrochemical Behavior of Thin Film Analogs of Mg(Zn, Cu, Al)₂. *J. Electrochem. Soc.* **2001**, *148*, B348. [[CrossRef](#)]
60. Lara-Banda, M.; Gaona-Tiburcio, C.; Zambrano-Robledo, P.; Delgado-E, M.; Cabral-Miramontes, J.A.; Nieves-Mendoza, D.; Maldonado-Bandala, E.; Estupiñan-López, F.; Chacón-Nava, J.G.; Almeraya-Calderón, F. Alternative to Nitric Acid Passivation of 15-5 and 17-4PH Stainless Steel Using Electrochemical Techniques. *Materials* **2020**, *13*, 2836. [[CrossRef](#)]
61. Montoya-Rangel, M.; de Oca, N.G.M.; Gaona-Tiburcio, C.; Colás, R.; Cabral-Miramontes, J.; Nieves-Mendoza, D.; Maldonado-Bandala, E.; Chacón-Nava, J.; Almeraya-Calderón, F. Electrochemical Noise Measurements of Advanced High-Strength Steels in Different Solutions. *Metals* **2020**, *10*, 1232. [[CrossRef](#)]
62. Ispas, A.; Bund, A.; Vrublevsky, I. Investigations on Current Transients in Porous Alumina Films during Re-Anodizing Using the Electrochemical Quartz Crystal Microbalance. *J. Solid State Electrochem.* **2010**, *14*, 2121–2128. [[CrossRef](#)]
63. Huang, Y.S.; Shih, T.S.; Chou, J.H. Electrochemical Behavior of Anodized AA7075-T73 Alloys as Affected by the Matrix Structure. *Appl. Surf. Sci.* **2013**, *283*, 249–257. [[CrossRef](#)]
64. Zaraska, L.; Gawlak, K.; Gurgul, M.; Dziurka, M.; Nowak, M.; Gilek, D.; Sulka, G.D. Influence of Anodizing Conditions on Generation of Internal Cracks in Anodic Porous Tin Oxide Films Grown in NaOH Electrolyte. *Appl. Surf. Sci.* **2018**, *439*, 672–680. [[CrossRef](#)]
65. Gawalt, E.S.; Brault-Rios, K.; Dixon, M.S.; Tang, D.C.; Schwartz, J. Enhanced Bonding of Organometallics to Titanium via a Titanium(III) Phosphate Interface. *Langmuir* **2001**, *17*, 6743–6745. [[CrossRef](#)]
66. Khudhair, D.; Bhatti, A.; Li, Y.; Hamedani, H.A.; Garmestani, H.; Hodgson, P.; Nahavandi, S. Anodization Parameters Influencing the Morphology and Electrical Properties of TiO₂ Nanotubes for Living Cell Interfacing and Investigations. *Mater. Sci. Eng. C* **2016**, *59*, 1125–1142. [[CrossRef](#)] [[PubMed](#)]
67. El-Taib Heakal, F.; Mogoda, A.S.; Mazhar, A.A.; El-Basiouny, M.S. Kinetic Studies on the Dissolution of the Anodic Oxide Film on Titanium in Phosphoric Acid Solutions. *Corros. Sci.* **1987**, *27*, 453–462. [[CrossRef](#)]
68. Parse, H.; Patil, I.M.; Swami, A.S.; Kakade, B.A. TiO₂-Decorated Titanium Carbide MXene Co-Doped with Nitrogen and Sulfur for Oxygen Electroreduction. *ACS Appl. Nano Mater.* **2021**, *4*, 1094–1103. [[CrossRef](#)]
69. Martinez, A.I.; Flamini, D.o.; Saidman, S.B. Corrosion Resistance Improvement of Ti-6Al-4V Alloy by Anodization in the Presence of Inhibitor Ions. *Trans. Nonferrous Met. Soc. China* **2022**, *32*, 1896–1909. [[CrossRef](#)]
70. Ramirez, A.; Gonzalez, J.; Campillo, B.; Gaona, T.; Dominguez, P.; Lezama, L.; Chacón, N.; Neri, F.; Martinez, V. An Electrochemical Study of the Corrosion Behavior of a Dual Phase Steel in 0.5M H₂SO₄. *Int. J. Electrochem. Sci.* **2010**, *5*, 1786–1798.
71. Fouda, M.E.; Allagui, A.; Elwakil, A.S.; Das, S.; Psychalinos, C.; Radwan, A.G. Nonlinear charge-voltage relationship in constant phase element. *Int. J. Electron. Commun. AEÜ* **2020**, *177*, 153104. [[CrossRef](#)]
72. Gomes, M.P.; Costa, I.; Pebere, N.; Rossi, J.L.; Tribollet, B.; Vivier, V. On the corrosion mechanism of Mg investigated by electrochemical impedance spectroscopy. *Electrochim. Acta* **2019**, *306*, 61–70. [[CrossRef](#)]
73. Gateman, S.M.; Gharbi, O.; Gomes de Melo, H.; Ngo, K.; Turmine, M.; Vivier, V. On the use of a constant phase element (CPE) in electrochemistry. *Curr. Opin. Electrochem.* **2022**, *36*, 101133. [[CrossRef](#)]

74. Barsoukov, E.; Macdonald, J.R. *Impedance Spectroscopy: Theory, Experiment, and Applications*, 3rd ed.; John Wiley & Sons, Inc: New York, NY, USA, 2018; pp. 175–478.
75. Macdonald, J.R. Frequency response of inifield dielectric and conductive systems involving an exponential distribution of activation energy. *J. Appl. Phys.* **1985**, *58*, 1955. [[CrossRef](#)]
76. Macdonald, J.R. Generalizations of “universal dielectric response” and a general distribution-of-activation-energies model for dielectric and conductive systems. *J. App. Phys.* **1985**, *58*, 1971. [[CrossRef](#)]
77. Mulder, W.H.; Sluyters, J.H.; Pajkossy, T.; Nyikos, L. Tafel current at fractal electrodes: Connection with admittance spectra. *J. Electroanal. Chem.* **1990**, *285*, 103. [[CrossRef](#)]
78. Kim, C.; Pyun, S.; Kim, J. An investigation of the capacitance dispersion on the fractal carbon electrode with edge and basal orientations, *Electrochim. Acta* **2003**, *48*, 3455. [[CrossRef](#)]
79. Schiller, C.A.; Strunz, W. The evaluation of experimental dielectric data of barrier coatings by means of different models. *Electrochim. Acta* **2001**, *46*, 3619. [[CrossRef](#)]
80. Córdoba-Torres, P. Relationship between constant-phase element (CPE) parameters and physical properties of films with a distributed resistivity. *Electrochim. Acta* **2017**, *225*, 592. [[CrossRef](#)]
81. Magar, H.S.; Hassan, R.Y.A.; Mulchandani, A. Electrochemical Impedance Spectroscopy (EIS): Principles, Construction, and Biosensing Applications. *Sensors* **2021**, Vol. 21, Page 6578 **2021**, *21*, 6578. [[CrossRef](#)] [[PubMed](#)]
82. Rajan, S.T.; V V, A.T.; Terada-Nakaishi, M.; Chen, P.; Hanawa, T.; Nandakumar, A.K.; Subramanian, B. Zirconium-Based Metallic Glass and Zirconia Coatings to Inhibit Bone Formation on Titanium. *Biomed. Mater.* **2020**, *15*, 065019. [[CrossRef](#)] [[PubMed](#)]
83. Kumar, P.; Mahobia, G.S.; Mandal, S.; Singh, V.; Chattopadhyay, K. Enhanced Corrosion Resistance of the Surface Modified Ti-13Nb-13Zr Alloy by Ultrasonic Shot Peening. *Corros. Sci.* **2021**, *189*, 109597. [[CrossRef](#)]
84. Radovanović, M.B.; Tasić, Ž.Z.; Simonović, A.T.; Petrović Mihajlović, M.B.; Antonijević, M.M. Corrosion Behavior of Titanium in Simulated Body Solutions with the Addition of Biomolecules. *ACS Omega* **2020**, *5*, 12768–12776. [[CrossRef](#)]
85. Vasilescu, C.; Drob, S.I.; Osiceanu, P.; Moreno, J.M.C.; Prodana, M.; Ionita, D.; Demetrescu, I.; Marcu, M.; Popovici, I.A.; Vasilescu, E. Microstructure, Surface Characterization, and Electrochemical Behavior of New Ti-Zr-Ta-Ag Alloy in Simulated Human Electrolyte. *Metall. Mater. Trans. A Phys. Metall. Mater. Sci.* **2017**, *48*, 513–523. [[CrossRef](#)]
86. Munirathinam, B.; Neelakantan, L. Titania Nanotubes from Weak Organic Acid Electrolyte: Fabrication, Characterization and Oxide Film Properties. *Mater. Sci. Eng. C* **2015**, *49*, 567–578. [[CrossRef](#)]
87. Cui, W.F.; Jin, L.; Zhou, L. Surface Characteristics and Electrochemical Corrosion Behavior of a Pre-Anodized Microarc Oxidation Coating on Titanium Alloy. *Mater. Sci. Eng. C* **2013**, *33*, 3775–3779. [[CrossRef](#)]
88. Sun, J.; Liu, Y. Unique Constant Phase Element Behavior of the Electrolyte–Graphene Interface. *Nanomaterials* **2019**, *9*, 923. [[CrossRef](#)]
89. Baltazar-Zamora, M.A.; Bandala, E.M.; Tello, M.U.; Hurtado, G.S.; Coca, F.J.; Cedano, A.O.; Barrios, C.P.; Nuñez, R.E.; Zambrano, P.; Tiburcio, C.; et al. Efficiency of Galvanized Steel Embedded in Concrete Previously Contaminated with 2, 3 and 4% of NaCl. *Int. J. Electrochem. Sci.* **2012**, *7*, 2997–3007.
90. Sadek, A.Z.; Zheng, H.; Latham, K.; Wlodarski, W.; Kalantar-Zadeh, K. Anodization of Ti Thin Film Deposited on ITO. *Langmuir* **2009**, *25*, 509–514. [[CrossRef](#)]
91. Mor, G.K.; Varghese, O.K.; Paulose, M.; Mukherjee, N.; Grimes, C.A. Fabrication of Tapered, Conical-Shaped Titania Nanotubes. *J. Mater. Res.* **2003**, *18*, 2588–2593. [[CrossRef](#)]
92. Galván-Martínez, R.; Cabrera-de la Cruz, D.; Contreras, A.; Orozco-Cruz, R. A novel experimental arrangement for corrosion study of X60 pipeline steel weldments at turbulent flow conditions. *Corros. Eng. Sci. Technol.* **2016**, *5*, 400–407. [[CrossRef](#)]
93. Galván-Martínez, R.; Orozco-Cruz, R.; Torres-Sanchez, R.; Martínez, E.A. Corrosion study of the X52 steel immersed in seawater with a corrosion inhibitor using a rotating cylinder electrode. *Mater. Corros.* **2010**, *61*, 872–876. [[CrossRef](#)]

Disclaimer/Publisher’s Note: The statements, opinions and data contained in all publications are solely those of the individual author(s) and contributor(s) and not of MDPI and/or the editor(s). MDPI and/or the editor(s) disclaim responsibility for any injury to people or property resulting from any ideas, methods, instructions or products referred to in the content.